

Short Communication

Liquid Crystal Template Assisted Electrodeposition of Molybdenum Sulfide Nanoparticles Supported on Carbon Fiber as Efficient Electrocatalyst for Hydrogen Evolution Reaction

Yong-Ming Chai¹, Xiao Shang¹, Wen-Kun Gao^{1,2}, Bin Dong^{1,2,*}, Chen-Guang Liu¹

¹ State Key Laboratory of Heavy Oil Processing, China University of Petroleum (East China), Qingdao 266580, PR China

² College of Science, China University of Petroleum (East China), Qingdao 266580, PR China

*E-mail: dongbin@upc.edu.cn

Received: 5 June 2017 / Accepted: 22 July 2017 / Published: 10 May 2018

Liquid crystal template (LCT) assisted electrodeposition has been utilized to prepare the amorphous MoS_x nanoparticles supported on carbon fiber (MoS_x/CF(LCT)) as electrocatalyst for hydrogen evolution reaction (HER). For comparison, MoS_x electrodeposited in water solution (MoS_x/CF(H₂O)) has also been obtained under the same condition. For both LCT and water solution, the as-deposited MoS_x shows similar amorphous structure, whereas LCT-derived MoS_x exhibits unique nanoparticles uniformly distributing on CF, compared with smooth plane structures of water solution-derived MoS_x. The unique LCT-derived MoS_x nanoparticles may be favorable for more exposure of active sites, improving the contact with electrolyte and accelerating charge transfer. Compared with MoS_x/CF(H₂O), MoS_x/CF(LCT) show superior HER activities as well as excellent stability in the electrochemical measurements. SEM images demonstrate the structural stability of MoS_x/CF(LCT) with nearly unchangeable nanoparticle morphology. Therefore, the LCT-assisted electrodeposition may provide a facile routine to obtain transition metal-based sulfides with unique nanostructure as well as excellent HER properties.

Keywords: electrodeposition; liquid crystal template; nanoparticle; molybdenum sulfide; hydrogen evolution reaction

1. INTRODUCTION

Water splitting has been regarded as an efficient access to hydrogen energy as renewable energy resources to resolve energy crisis and environmental depletion from fossil fuels [1-7]. The overall efficiency of water splitting relies on efficient electrocatalysts to accelerate hydrogen evolution

reaction (HER) process of water splitting. So far, Pt-based materials are the best catalysts for HER, whereas the scarcity and expensiveness hinder their wide applications [8-10]. Great efforts have been devoted on selecting earth abundant materials such as transition metals and their derivatives, and molybdenum sulfide have received many attentions due to the cost-effective nature and excellent properties [11-14].

It has been acknowledged that the HER activity of MoS_x are determined by the rims and edges, whereas the basal plane remains chemically inert [15, 16]. One strategy to expose the rims and edges is fabricating various nanostructured MoS_x , such as defect-rich structures [17], hollow nanospheres [18], vertical nanoflakes [19] or mesoporous films [20]. Moreover, in order to avoid the stacking of layered MoS_x nanostructure as well as enhance the conductivity, many supports such as carbon-based materials have been adopted to effectively disperse the active species [21-23]. Carbon fiber (CF) has recently emerged as a new type of three-dimensional (3D) substrate with low cost, high conductivity and flexibility, which holds promising as ideal substrate to load active species for HER [24, 25].

On the other hand, it still remains challengeable to fabricate unique MoS_x nanostructures in a facile way. Most of the methods require harsh conditions like high temperature and complicated procedures. It is significant to develop a facile and green synthesis to prepare MoS_x -based electrocatalysts with enhanced HER activity. Recently, electrodeposition has been highly attractive due to its mild and facile merits to control the growth of amorphous MoS_x species in room temperature [26, 27]. Furthermore, the unique nanostructures of MoS_x can be realized by employing ionic liquids or liquid crystal template (LCT) as the electrodeposition electrolyte to expose abundant active sites for HER [28, 29]. The utilization of LCT as special electrolyte has previously proved to be a simple way to obtain various nanostructured materials in electrodeposition process [30-32]. Thus it is expected that the LCT-derived MoS_x may also possess unique nanostructure with attractive electrochemical properties.

Herein, LCT has been employed as electrolyte in electrodeposition of amorphous MoS_x nanoparticles on the CF as support ($\text{MoS}_x/\text{CF}(\text{LCT})$). For comparison, MoS_x has also been electrodeposited merely in water solution ($\text{MoS}_x/\text{CF}(\text{H}_2\text{O})$) under the same condition. The LCT is a uniform liquid mixture composed of nonionic surfactants (Triton X-100) and MoS_x sources in certain mass ratio. The XRD and XPS characterizations have demonstrated similar amorphous nanostructure of LCT-derived and water solution-derived MoS_x species. However, SEM images show that LCT-derived MoS_x has unique nanoparticles in similar sizes distributing on the surface of CF, compared with smooth plane MoS_x structures electrodeposited from water solution. The unique MoS_x nanoparticle of $\text{MoS}_x/\text{CF}(\text{LCT})$ may expose abundant active sites for HER, improve the contact of electrolyte and facilitate charge transfer. The electrochemical measurements show the enhanced HER activities of $\text{MoS}_x/\text{CF}(\text{LCT})$ than $\text{MoS}_x/\text{CF}(\text{H}_2\text{O})$, demonstrating the advantageous LCT-derived nanoparticle structures. The $\text{MoS}_x/\text{CF}(\text{LCT})$ also possesses structural stability in the stability test with nearly unchangeable nanoparticle structures. It may provide a facile access to transition metal-based materials with excellent HER performances.

2. EXPERIMENTAL SECTION

2.1 Preparation of $\text{MoS}_x/\text{CF}(\text{H}_2\text{O})$ and $\text{MoS}_x/\text{CF}(\text{LCT})$

Prior to the preparation, carbon fiber (CF) with size of $1 \times 2 \text{ cm}^2$ was consecutively sonicated in acid, acetone and ethanol for 20 min consecutively. Then it was dried in vacuum at $60 \text{ }^\circ\text{C}$ for 8 h.

The preparation of $\text{MoS}_x/\text{CF}(\text{H}_2\text{O})$ and $\text{MoS}_x/\text{CF}(\text{LCT})$ was electrodeposited in the three-electrode system (Gamry Reference 600, USA) through cyclic voltammogram (CV). The pre-cleaned CF was used as working electrode, a carbon rod as counter electrode and a Ag/AgCl (saturated KCl) as reference. The potential window for electrodeposition was from -1.0 V to 0.1 V (vs. Ag/AgCl) at scan rate of 10 mV s^{-1} for 5 cycles. The electrodeposition electrolyte for $\text{MoS}_x/\text{CF}(\text{H}_2\text{O})$ was 5 mM $(\text{NH}_4)_2(\text{MoS}_4)$ at $50 \text{ }^\circ\text{C}$. For $\text{MoS}_x/\text{CF}(\text{LCT})$, the electrolyte was the uniform liquid crystal template containing 5 mM $(\text{NH}_4)_2(\text{MoS}_4)$ (52 wt.%) and Triton X-100(48 wt.%) at $50 \text{ }^\circ\text{C}$.

2.2 Physical characterization

X-ray powder diffraction (XRD) was conducted on X'Pert PRO MPD with Cu KR to investigate crystalline structures of samples. Scan electron microscopy (SEM) was employed on as-prepared samples utilizing Hitachi (S-4800). X-ray photoelectron spectra (XPS) data was collected on VG ESCALAB MK II with Al Ka (1486.6 eV) as photon source.

2.3 Electrochemical tests

Electrochemical tests were carried out on an electrochemical work station (Gamry Reference 600, USA) with a three-electrode system (three samples as working electrodes, a Pt foil as counter electrode and a Ag/AgCl (saturated KCl) as reference). The electrolyte was 0.5 M H_2SO_4 solution which was previously purified by nitrogen for 0.5 h. Linear sweep voltammetry (LSV) was undertaken with scan rate was 5 mV s^{-1} . Electrochemical impedance spectroscopy (EIS) was performed at -0.1 V (vs. Ag/AgCl) from 10^5 Hz to 10^{-2} Hz with an AC voltage of 5 mV . CV was utilized to test stability of $\text{MoS}_x/\text{CF}(\text{LCT})$ from -0.1 V to -0.5 V (vs. Ag/AgCl) for 500 cycles with scan rate of 100 mV s^{-1} .

3. RESULTS AND DISCUSSION

Figure 1 shows XRD patterns of all samples. It can be seen that all as-prepared samples contains peaks belonging to carbon fiber (96-210-3201). Besides, no other peaks can be found on $\text{MoS}_x/\text{CF}(\text{H}_2\text{O})$ and $\text{MoS}_x/\text{CF}(\text{LCT})$ from molybdenum sulfides, implying the amorphous nature of as-prepared deposits from water solution or LCT.

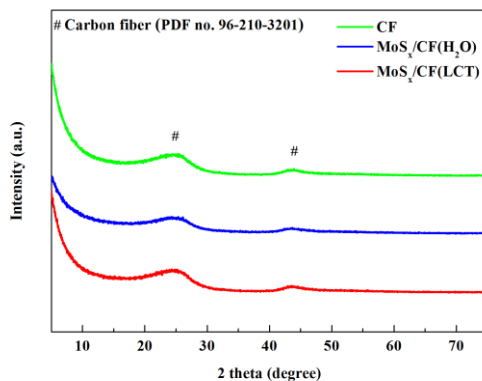
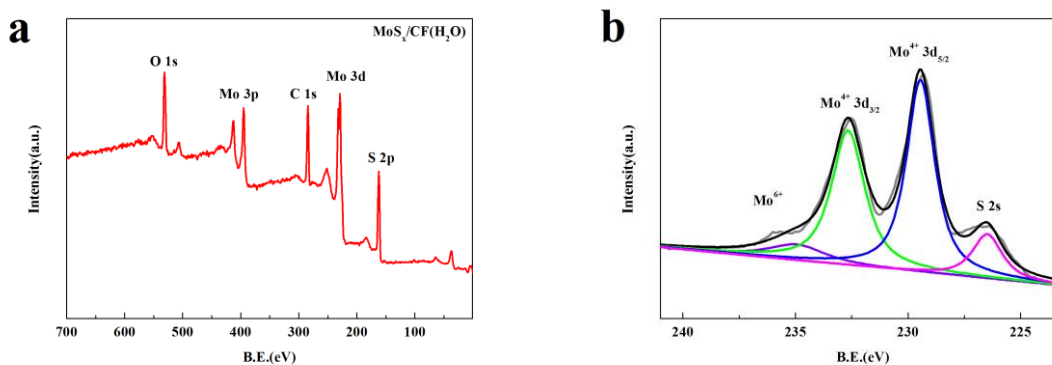


Figure 1. XRD patterns of CF, MoS_x/CF(H₂O) and MoS_x/CF(LCT).

The XPS data of MoS_x/CF(H₂O) and MoS_x/CF(LCT) are displayed in Figure 2 and Figure 3, respectively. In Figure 2a and Figure 3a, the XPS surveys show the existence of Mo and S, suggesting the successful electrodeposition of molybdenum sulfides. In addition, the detection of C and O may be largely derived from surface oxidation or contamination [33]. For Mo 3d region in Figure 2b and Figure 3b, the two characteristic peaks at 232.7 eV and 229.6 eV can be indexed to Mo 3d_{3/2} and Mo 3d_{5/2} of Mo(IV), respectively [22]. In addition, the higher oxidation state of Mo(VI) can also be detected at 235.6 eV derived from MoS₃ [34]. In Figure 2c and Figure 3c, the peaks at 161.3 eV and 162.5 eV are from S 2p_{3/2} and S 2p_{1/2}, respectively [35, 36]. The detection of S₂²⁻ at 164.4 eV demonstrates the formation of MoS₃, which is consistent with Figure 2b and Figure 3b [37]. On the above analysis of XPS data, it suggests the similar chemical states of MoS_x/CF(H₂O) and MoS_x/CF(LCT) which are not affected by different electrolyte of H₂O and LCT.

The surficial morphologies of MoS_x/CF(H₂O) and MoS_x/CF(LCT) are displayed in Figure 4. The pre-cleaned CF in Figure 4a shows interlaced carbon fibers with a smooth surface in the insertion. The surface of as-prepared MoS_x/CF(H₂O) (Figure 4b and Figure 4c) are covered by deposits in smooth plane structures, which is similar with our previous work [28, 38].



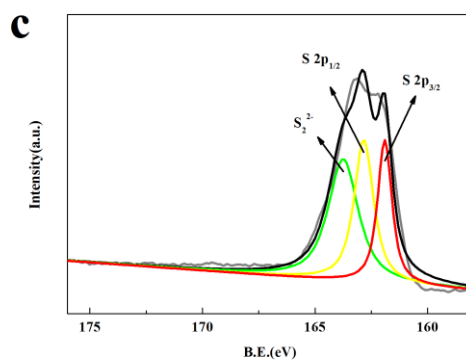


Figure 2. XPS spectra of MoS_x/CF(H₂O): (a) survey, (b) Mo 3d and (c) S 2p.

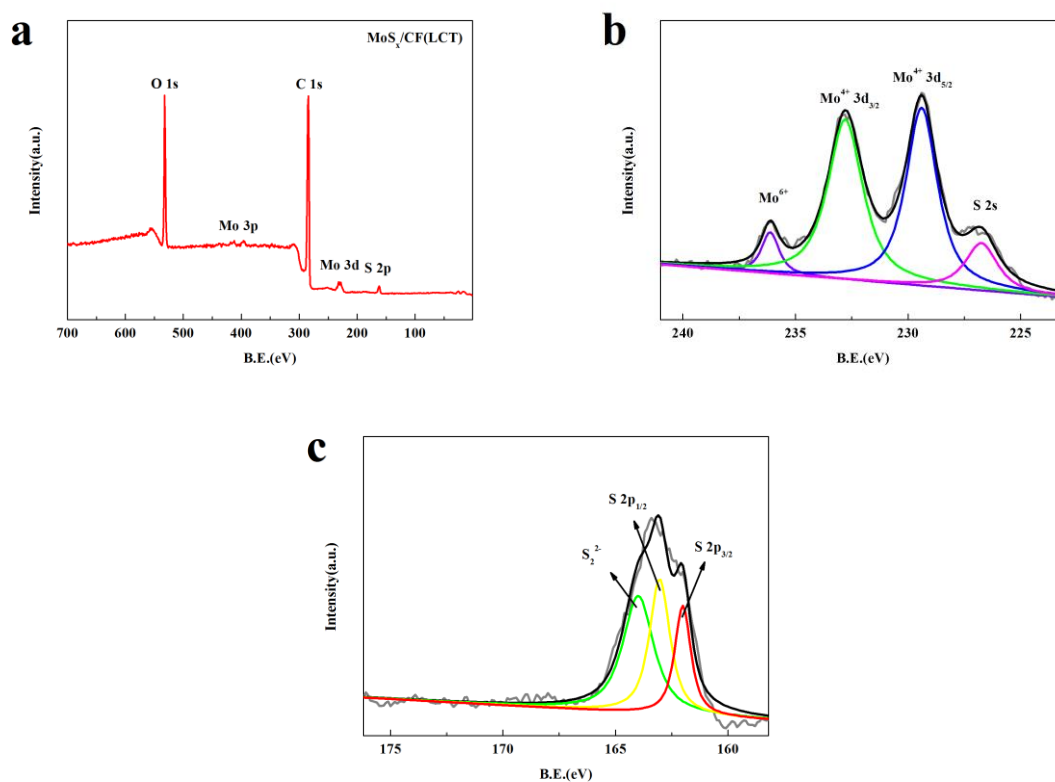
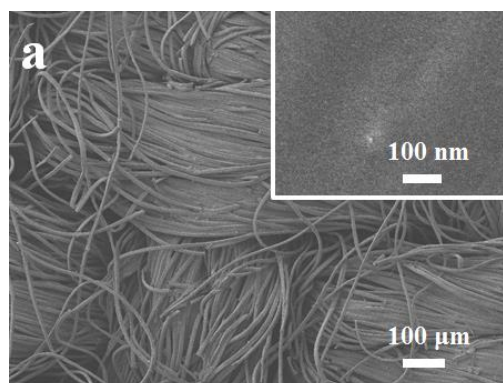


Figure 3. XPS spectrum of MoS_x/CF(LCT): (a) survey, (b) Mo 3d and (c) S 2p.



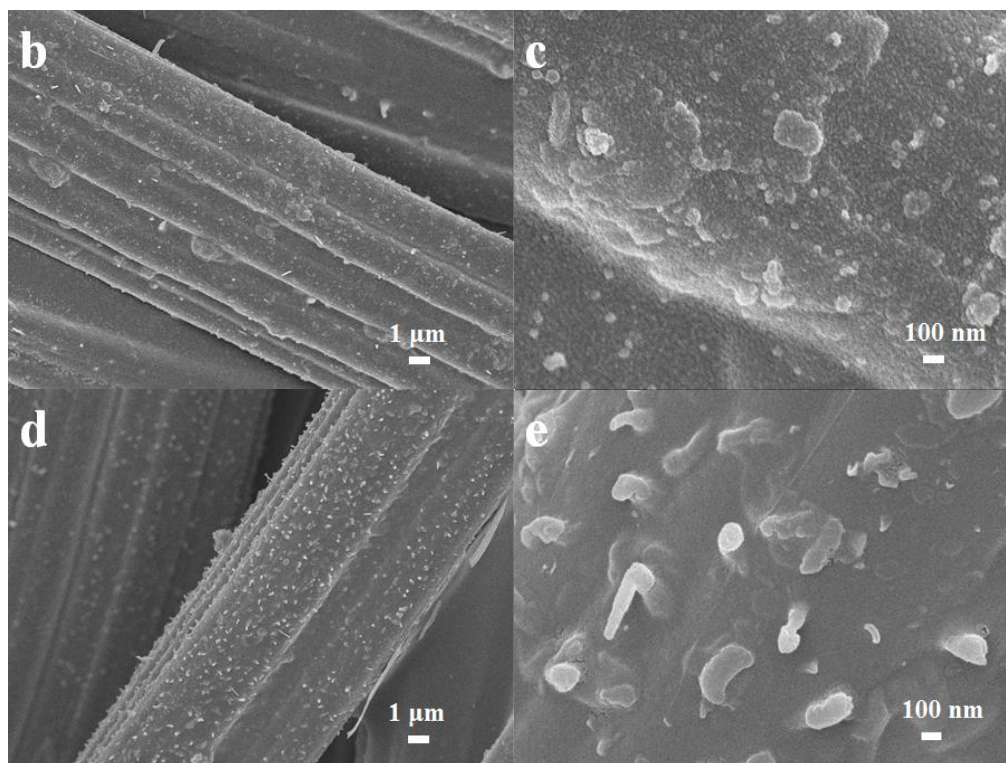


Figure 4. SEM images. (a) Bare CF. (b, c) MoS_x/CF(H₂O). (d, e) MoS_x/CF(LCT).

For LCT-derived MoS_x/CF(LCT) in Figure 4d and Figure 4e, the surface of CF are composed of many small nanoparticles in uniform sizes of 100-200 nm. The unique nanoparticle structures of MoS_x may be derived from controlling morphologies of LCT [28]. It may contain more rims and edges and expose more active sites for HER.

The HER activities of MoS_x/CF(H₂O) and MoS_x/CF(LCT) in 0.5 M H₂SO₄ are displayed in Figure 5. For comparison, the commercial Pt/C is also measured. In the LSV curves of Figure 5a, Pt/C shows the best HER activity with onset potential close to zero. In contrast, the bare CF has poor HER activity requiring large overpotentials to reach visible current densities. For MoS_x/CF(H₂O) and MoS_x/CF(LCT), the overpotential to deliver 10 mA cm⁻² are observed to be 378 and 247 mV, respectively. It illustrates the superior HER activity of MoS_x/CF(LCT) than MoS_x/CF(H₂O), which may be due to the unique LCT-derived nanoparticle structure with more exposed active sites [28]. The HER kinetics has been compared by Tafel plots shown in Figure 5b. The sample of MoS_x/CF(LCT) shows the Tafel slope of 45 mV dec⁻¹ indicative of the Volmer-Heyrovsky mechanism for HER [39], which is smaller than that (136 mV dec⁻¹) of MoS_x/CF(H₂O). It illustrates the improved HER reaction kinetics of LCT-derived MoS_x. The kinetics of HER in acid has been further investigated by electrochemical impedance spectroscopy (EIS), as shown in the Nyquist plots of Figure 5c. The MoS_x/CF(LCT) electrode owns the smallest the diameter than MoS_x/CF(H₂O), illustrating the enhanced conductivity and fast transfer rate. Therefore, the enhanced HER activity of MoS_x/CF(LCT) than MoS_x/CF(H₂O) can be attributed to the LCT-derived MoS_x nanoparticle morphology. First, the nanoparticle structure may enlarge the surface area, avoid aggregation and expose abundant active sites

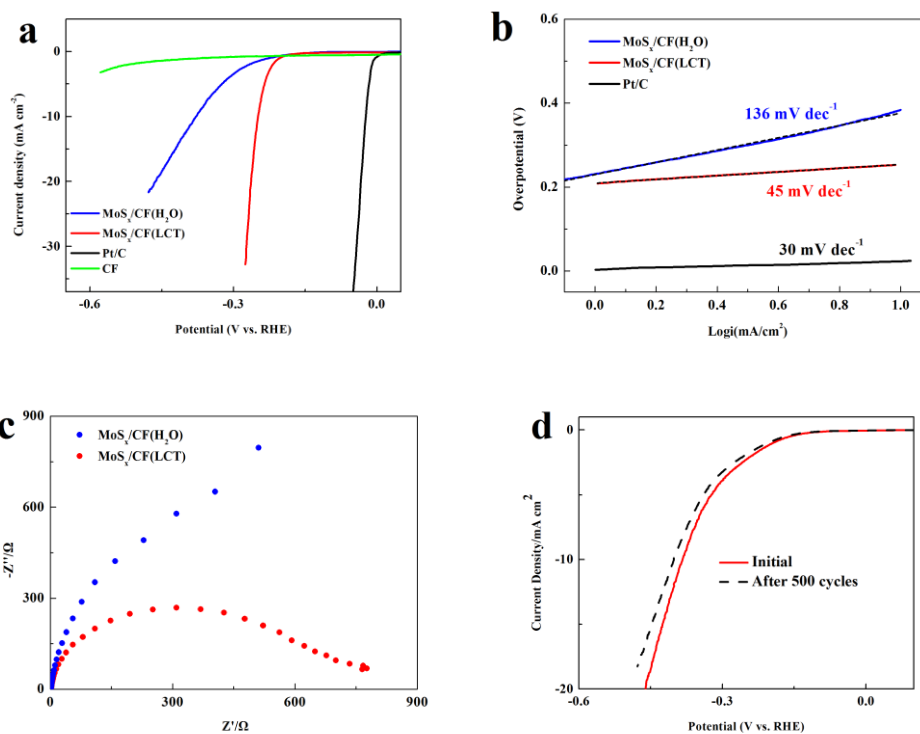


Figure 5. Electrochemical measurements: (a) LSV, (b) Tafel plots, (c) EIS, (d) stability test of $\text{MoS}_x/\text{CF}(\text{LCT})$.

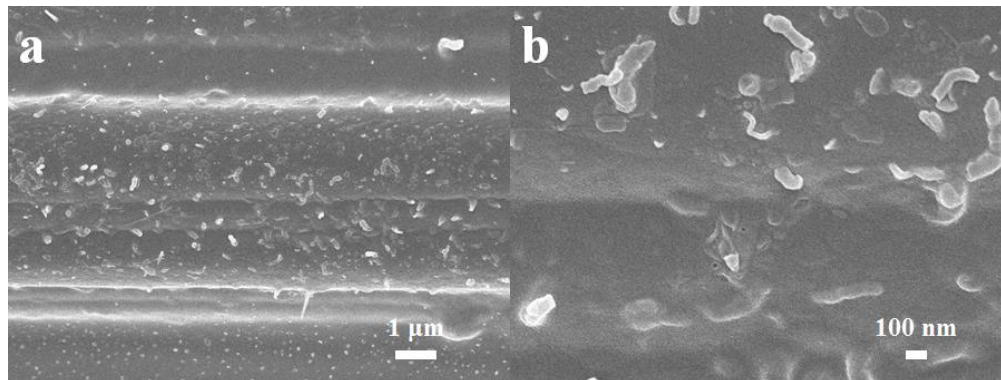


Figure 6. (a, b) SEM images of $\text{MoS}_x/\text{CF}(\text{LCT})$ after stability test.

for HER [29]. Besides, the uniform distribution of MoS_x nanoparticles on the surface of CF may enlarge the contacting in the catalyst/electrolyte interfaces and improve the charge transfer rate. The stability of $\text{MoS}_x/\text{CF}(\text{LCT})$ has been studied by CV for 500 cycles, as shown in Figure 5d. It can be seen that the current density of LSV decline a little after 500 cycles, suggesting that the HER activity are highly remained in long-term water electrolysis. The morphology of $\text{MoS}_x/\text{CF}(\text{LCT})$ after stability test is shown in Figure 6. In Figure 6a, the surface of CF are still covered by small nanoparticles with uniform distribution. A closer view in Figure 6b shows that part of nanoparticles become irregular, suggesting the inevitable destruct in long-term HER process.

4. CONCLUSIONS

In summary, we have utilized special LCT as electrolyte for electrodeposition to obtain MoS_x nanoparticles supported on carbon fiber (MoS_x/CF(LCT)). MoS_x has been also electrodeposited in water solution (MoS_x/CF(H₂O)) under the same condition. The XRD and XPS characterizations have exhibited similar amorphous nature of MoS_x in MoS_x/CF(H₂O) and MoS_x/CF(LCT). Differently, LCT-derived MoS_x are composed of small nanoparticles with uniform distribution, while water solution-derived MoS_x shows smooth plane structures. The unique nanoparticles on MoS_x/CF(LCT) may expose more active sites for HER, improve the contact of catalyst/electrolyte interfaces as well as the conductivity. The electrochemical measurements demonstrate the enhanced HER properties of MoS_x/CF(LCT) than MoS_x/CF(H₂O), which may be due to LCT-derived nanoparticle structures. The MoS_x/CF(LCT) possesses structural stability after stability test with unchangeable nanoparticle structures. It may provide a facile approach to transition metal-based electrocatalysts with excellent HER performances.

ACKNOWLEDGEMENTS

This work is financially supported by the Fundamental Research Funds for the Central Universities (15CX05031A).

References

1. Z.W. Seh, J. Kibsgaard, C.F. Dickens, I. Chorkendorff, J.K. Nørskov and T.F. Jaramillo, *Science*, 355 (2017) 6321.
2. X. Li, X. Shang, Y. Rao, B. Dong, G.Q. Han, W.H. Hu, Y.R. Liu, K.L. Yan, J.Q. Chi, Y.M. Chai and C.G. Liu, *Appl. Surf. Sci.*, 396 (2017) 1034.
3. X. X. Zou and Y. Zhang, *Chem. Soc. Rev.*, 44 (2015) 5148.
4. Y. Shi and B. Zhang, *Chem. Soc. Rev.*, 45 (2016) 1529.
5. J.Q. Chi, K.L. Yan, W.K. Gao, B. Dong, X. Shang, Y.R. Liu, X. Li, Y.M. Chai and C.G. Liu, *J. Alloys Compd.*, 714 (2017) 26.
6. W.J. Zhou, J. Jia, J. Lu, L. Yang, D. Hou, G. Li and S. Chen, *Nano Energy*, 28 (2016) 29.
7. Q. Ding, B. Song, P. Xu and S. Jin, *Chem*, 1(2016) 699.
8. Y. Liu, X. Shang, W.-K. Gao, B. Dong, X. Li, X. Li, J. Zhao, Y. Chai, Y. Liu and C. Liu, *J. Mater. Chem. A*, 5 (2017) 2885.
9. Y.-R. Liu, W.-H. Hu, X. Li, B. Dong, X. Shang, G.-Q. Han, Y.-M. Chai, Y.-Q. Liu and C.-G. Liu, *Appl. Surf. Sci.*, 383 (2016) 276.
10. B. Dong, W. H. Hu, G. Q. Han, Y. M. Chai and C. G. Liu, *Materials Review*, 30 (8A) (2016) 39.
11. W.-H. Hu, R. Yu, G.-Q. Han, Y.-R. Liu, B. Dong, Y.-M. Chai, Y.-Q. Liu and C.-G. Liu, *Mater. Lett.* 161 (2015) 120.
12. X. Shang, W.-H. Hu, X. Li, B. Dong, Y.-R. Liu, G.-Q. Han, Y.-M. Chai and C.-G. Liu, *Electrochim. Acta*, 224 (2017) 25.
13. W.-H. Hu, G.-Q. Han, F.-N. Dai, Y.-R. Liu, X. Shang, B. Dong, Y.-M. Chai, Y.-Q. Liu and C.-G. Liu, *Int. J. Hydrogen Energy*, 41 (2016) 294.
14. Y.-R. Liu, W.-H. Hu, X. Li, B. Dong, X. Shang, G.-Q. Han, Y.-M. Chai, Y.-Q. Liu and C.-G. Liu, *Appl. Surf. Sci.*, 384 (2016) 51.
15. T. F. Jaramillo, K. P. Jørgensen, J. Bonde, J. H. Nielsen, S. Horch and I. Chorkendorff, *Science*, 317

- (2007) 100.
16. B. Lassalle-Kaiser, D. Merki, H. Vrubel, S. Gul, V. K. Yachandra, X. Hu and J. Yano, *J. Am. Chem. Soc.*, 137 (2014) 314.
 17. J. Xie, H. Zhang, S. Li, R. Wang, X. Sun, M. Zhou, J. Zhou, X. W. D. Lou and Y. Xie, *Adv. Mater.*, 25 (2013) 5807.
 18. B. Guo, K. Yu, H. Li, H. Song, Y. Zhang, X. Lei, H. Fu, Y. Tan and Z. Zhu, *ACS Appl. Mater. Interfaces*, 8 (2016) 5517.
 19. D. Kong, H. Wang, J. J. Cha, M. Pasta, K. J. Koski, J. Yao and Y. Cui, *Nano Lett.*, 13 (2013) 1341.
 20. J. Bonde, P. G. Moses, T. F. Jaramillo, J. K. Nørskov and I. Chorkendorff, *Faraday Discuss.*, 140 (2009) 219.
 21. W.-H. Hu, X. Shang, J. Xue, B. Dong, J.-Q. Chi, G.-Q. Han, Y.-R. Liu, X. Li, K.-L. Yan, Y.-M. Chai and C.-G. Liu, *Int. J. Hydrogen Energy*, 42 (2017) 2088.
 22. W.-H. Hu, X. Shang, G.-Q. Han, B. Dong, Y.-R. Liu, X. Li, Y.-M. Chai, Y.-Q. Liu and C.-G. Liu, *Carbon*, 100 (2016) 236.
 23. W.-H. Hu, G.-Q. Han, Y.-R. Liu, B. Dong, Y.-M. Chai, Y.-Q. Liu and C.-G. Liu, *Int. J. Hydrogen Energy*, 40 (2015) 6552.
 24. X. Shang, K.-L. Yan, Z.-Z. Liu, S.-S. Lu, B. Dong, J.-Q. Chi, X. Li, Y.-R. Liu, Y.-M. Chai and C.-G. Liu, *Appl. Surf. Sci.*, 402 (2017) 120.
 25. X. Shang, J.-Q. Chi, S.-S. Lu, B. Dong, X. Li, Y.-R. Liu, K.-L. Yan, W.-K. Gao, Y.-M. Chai and C.-G. Liu, *Int. J. Hydrogen Energy*, 42 (2017) 4165.
 26. D. Merki, S. Fierro, H. Vrubel and X. Hu, *Chem. Sci.*, 2 (2011) 1262.
 27. D. Merki, H. Vrubel, L. Rovelli, S. Fierro and X. Hu, *Chem. Sci.*, 3 (2012) 2515.
 28. G.-Q. Han, X. Shang, S.-S. Lu, B. Dong, X. Li, Y.-R. Liu, W.-H. Hu, J.-B. Zeng, Y.-M. Chai and C.-G. Liu, *Int. J. Hydrogen Energy*, 42 (2017) 5132.
 29. S. Murugesan, A. Akkineni, B. P. Chou, M. S. Glaz, D. A. Vanden Bout and K. J. Stevenson, *ACS Nano*, 7 (2013) 8199.
 30. B. Dong, T. Xue, C.-L. Xu and H.-L. Li, *Micropor. Mesopor. Mat.*, 112 (2008) 627.
 31. G. S. Attard, P. N. Bartlett, N. R. Coleman, J. M. Elliott, J. R. Owen and J. H. Wang, *Science*, 278 (1997) 838.
 32. L. Huang, H. Wang, Z. Wang, A. Mitra, K. N. Bozhilov and Y. Yan, *Adv. Mater.*, 14 (2002) 61.
 33. A. Panneerselvam, M. A. Malik, M. Afzaal, P. O'Brien and M. Helliwell, *J. Am. Chem. Soc.*, 130 (2008) 2420.
 34. X. Zheng, J. Xu, K. Yan, H. Wang, Z. Wang and S. Yang, *Chemistry of Materials*, 26 (2014) 2344-2353.
 35. A. De Jong, H. Borg, L. Van IJzendoorn, V. Soudant, V. De Beer, J. Van Veen and J. Niemantsverdriet, *J. Phys. Chem.*, 97 (1993) 6477.
 36. M. Xu, F. Yi, Y. Niu, J. Xie, J. Hou, S. Liu, W. Hu, Y. Li and C. M. Li, *J. Mater. Chem. A*, 3 (2015) 9932.
 37. Y.-H. Chang, R. D. Nikam, C.-T. Lin, J.-K. Huang, C.-C. Tseng, C.-L. Hsu, C.-C. Cheng, C.-Y. Su, L.-J. Li and D. H. Chua, *ACS Appl. Mater. Interfaces*, 6 (2014) 17679.
 38. G.-Q. Han, X. Li, J. Xue, B. Dong, X. Shang, W.-H. Hu, Y.-R. Liu, J.-Q. Chi, K.-L. Yan and Y.-M. Chai, *Int. J. Hydrogen Energy*, 42 (2017) 2952.
 39. C. G. Morales-Guio, L.-A. Stern and X. Hu, *Chem. Soc. Rev.*, 43 (2014) 6555